

Excitonic instability in transition metal dichalcogenides

M. F. C. Martins Quintela^{1,2}, A. T. Costa², N. M. R. Peres^{1,2}

¹Department of Physics and Centre of Physics of the Universities of Minho and Porto (CF-UM-UP), Campus of Gualtar, 4710-057, Braga, Portugal

²International Iberian Nanotechnology Laboratory (INL), Av. Mestre José Veiga, 4715-330, Braga, Portugal

E-mail: mfcquintela@gmail.com

Abstract. When transition-metal dichalcogenide monolayers lack inversion symmetry, their low-energy single particle spectrum can be described by tilted massive Dirac Hamiltonians. The so-called Janus materials fall into that category. Inversion symmetry can also be broken by the application of out-of-plane electric fields, or by the mere presence of a substrate. Here we explore the properties of excitons in TMDC monolayers lacking inversion symmetry. We find that exciton binding energies can be larger than the electronic band gap, making such materials promising candidates to host the elusive exciton insulator phase. We also investigate the excitonic contribution to their optical conductivity and discuss the associated optical selection rules.

Keywords: Janus, TMD, exciton, monolayer, conductivity, tilted Dirac cone

Submitted to: *J. Phys.: Condens. Matter*

1. Introduction

Janus transition metal dichalcogenide (TMD) monolayers are a new type of two-dimensional materials, recently synthesized [1, 2] in the form of MoSSe. In this material, one atomic layer of Mo is encapsulated by two different chalcogen layers, namely S and Se. This creates an asymmetry in the direction perpendicular to the plane of the structure, resulting in a dipole moment pointing from the Se to the S layer [3, 4]. These first two independent experiments [1, 2] triggered a large wave of theoretical studies[5] into the electronic band structure[2], anisotropic elasticity and transport[6], as well as piezoelectric [7], pyroelectric [8], spin [9], and photocarrier [10] properties of Janus structures. Additionally, several potential applications have been studied, such as in water splitting [11], gas sensing [12], and photovoltaics [13].

The band structure and the Berry curvature dipole [14, 15, 16] of Janus TMD monolayers are well described by a tilted massive Dirac model [17, 18, 19]. For instance, this two-band effective model captures the pronounced peak in the dipole component near the Fermi level of $T'-WSe_2$, seen in DFT calculations [17]. This feature is a consequence of a reduced band gap, which leads to a large Berry curvature [17]. Tilted Dirac cones are also seen in 8 - $Pmmn$ borophene [20, 21, 22], where the low-energy regime near the Dirac points can be accurately described via an effective anisotropic tilted Hamiltonian [20, 21, 23, 24].

Several properties of systems with tilted massive Dirac Hamiltonians have been studied, such as anomalous spin transport[25], topological properties[26], photoinduced anomalous [27] and nonlinear Hall effects [18], quantum criticality [28], chiral excitonic instabilities [29], and orbital-selective photoexcitation [30]. Additionally, the importance of spin-orbit coupling in layered organic salts has also been studied via a Hamiltonian with tilted band structure [31, 32]. Explicit inversion symmetry breaking and anisotropic terms are also present in other families of materials, such as Weyl semimetals [33] with broken tilt inversion symmetry, where second harmonic generation has been recently studied [34], and type-II semi-Dirac semimetals [35, 36, 37], where it has been shown that

linear and nonlinear anomalous Hall effects can be manipulated via circularly polarized light [38].

A defining feature of massive tilted Dirac cones is the tunability of their electronic band gap, illustrated in Fig. (1). By tuning a single parameter, it is possible to go from a direct gap semiconductor to a metal, passing through an indirect gap semiconductor and a semi-metal. *Ab initio* calculations [39] suggest that such tunability can be achieved in real materials by the application of an out-of-plane electric field. Thus, materials that host massive tilted Dirac cones are especially attractive as platforms on which new electronic phases can be found. One such phase is the excitonic insulator, first predicted qualitatively by Mott in 1961 [40]. The concept has been subsequently refined and put on firmer grounds by several authors [41, 42, 43, 44]. In brief, when the binding energy of excitons surpasses the value of the electronic band gap, the system becomes unstable against a proliferation of excitons[45]. The true ground state of such a system is an “exciton condensate”, akin in many ways to the Cooper pair condensate found in superconductors[43]. This analysis apply equally to small gap semiconductors and semimetals, provided the overlap between conduction and valence bands is small, such that screening of the Coulomb interaction between electrons and holes is negligible. Although predicted more than 60 years ago, the excitonic insulator has eluded conclusive experimental observation until very recently. One of the main difficulties is that the excitonic instability is frequently accompanied by structural instabilities, associated with the softening of phonon modes, which are hard to disentangle from the former.

Here we look into the properties of excitons in 2D massive tilted Dirac electrons. We show that the band gap can be tuned while the exciton binding energy remains constant, moving the system towards an excitonic instability. Importantly, as the magnitude of the gap decreases, the maximum of the valence band and the minimum of the conduction band shift in opposite directions in reciprocal space, making the gap indirect. This guarantees that the dielectric function of the material remains finite even as the gap approaches zero, and the exciton binding energies are not strongly affected by the smallness of the

gap[41]. It is also noteworthy that the excitonic contribution to the conductivity is insensitive to the tilting parameter; thus, at least in principle, one can expect a sudden change in transport properties as the excitonic instability is reached by tuning of the tilting parameter.

This paper is structured as follows. In Sec. 2, we discuss the tilted Dirac Hamiltonian [18], illustrating the features induced by the tilt parameter on the single particle electronic eigenstates and band structure. In Sec. 3, we introduce the Bethe-Salpeter equation, briefly discussing the electrostatic potential coupling different bands. The screening length of the material is also introduced, and the influence of the tilt parameter on the excitonic states is analyzed. Finally, the optical selection rules and oscillator strengths are discussed, and the excitonic optical conductivity is computed.

2. Tilted Dirac Hamiltonian

The effective two-band tilted Dirac Hamiltonian has been shown to capture the essential features of both the low-energy band structure and the Berry curvature dipole moment of Janus TMD monolayers, such as WTe [17]. This Hamiltonian includes an anisotropic term which preserves time-reversal symmetry but explicitly breaks inversion symmetry, tilting the band structure in a specific direction, here considered to be the x -axis. The Hamiltonian can therefore be written as [16, 17, 18]

$$\hat{\mathcal{H}}_d = tk^x\sigma_0 + v(k^y\sigma_x + \eta k^x\sigma_y) + (m/2 - \alpha k^2)\sigma_z, \quad (1)$$

where (k_x, k_y) are the wave vectors, $k^2 = k_x^2 + k_y^2$, $(\sigma_x, \sigma_y, \sigma_z)$ are the Pauli matrices, σ_0 is the 2×2 identity matrix, $\eta = \pm 1$ is a valley-like index, m is the gap, and t tilts the Hamiltonian in the x direction. In Eq. (1), the α parameter is introduced to regulate topological properties as $k \rightarrow \infty$ [46]. For clarity, we also write this Hamiltonian in matrix form, where it is given by

$$\hat{\mathcal{H}}_d = \begin{bmatrix} tk_x + (\frac{m}{2} - \alpha k^2) & -iv(\eta k_x + ik_y) \\ iv(\eta k_x - ik_y) & tk_x - (\frac{m}{2} - \alpha k^2) \end{bmatrix}. \quad (2)$$

The band dispersion of this model is given by

$$E_\lambda(k) = tk_x + \lambda\sqrt{k^2v^2 + (m/2 - \alpha k^2)^2}, \quad (3)$$

with $\lambda = \pm 1$ the conduction/valence band index. Choosing $\eta = -1$ as in [17, 18], the (non-normalized) eigenvectors are given by

$$\begin{aligned} |u_+(k, \theta)\rangle &= \begin{bmatrix} i \frac{m - 2\alpha k^2 + \lambda\sqrt{k^2v^2 + (m/2 - \alpha k^2)^2}}{2kv} \\ e^{i\theta} \end{bmatrix}, \\ |u_-(k, \theta)\rangle &= \begin{bmatrix} ie^{-i\theta} \frac{m - 2\alpha k^2 + \lambda\sqrt{k^2v^2 + (m/2 - \alpha k^2)^2}}{2kv} \\ 1 \end{bmatrix}, \end{aligned} \quad (4)$$

where $\theta = \arctan(k_y/k_x)$. By inspection of both Eq. (3) and Eq. (4) it is immediately clear that the tilt parameter t influences neither the difference between the two bands (*i.e.*, $E_+(k) - E_-(k)$) nor the eigenstates of the Hamiltonian. Its only effect is to produce a tilt of the dispersion relation along the x -axis. In Fig. 1 we show the dispersion relation for a few representative values of t . The other parameters have been chosen as $v = 1 \text{ eV\AA}$, $\alpha = 1 \text{ eV\AA}^2$ and $m = 0.2 \text{ eV}$ [18]. For $t = 0$ (top left) there is a gap at $k = 0$, which is continuously suppressed as $t \rightarrow v$. Notice also that, for any $0 < t < v$, the gap becomes indirect. For $t/v \geq 1$ (bottom panels) the model describes a semimetal with zero ($t = v$) or small $t/v \gtrsim 1$ carrier density.

In Fig. (2), we plot the Fermi rings at a Fermi energy of $E_F = m/2$ for various values of t/v . The top of the valence band crosses the $E = \frac{m}{2}$ plane at roughly $t/v \approx 1.245$, as can be seen from the sudden appearance of the Fermi ring regarding this band. The anisotropy introduced by the tilt of the bands along the k_x axis is also clear when compared with the full symmetry along the k_y axis.

3. Excitons in tilted Dirac materials

We now look at the excitons of the massive tilted Dirac fermion model. Our approach is to solve the Bethe-Salpeter equation (BSE). As neither the difference between the two bands nor the eigenvectors depend on t , we do not expect this parameter to play a part in the excitonic properties of the system.

3.1. Solving the Bethe-Salpeter equation

The Bethe-Salpeter equation can be written in momentum space as [47, 48, 49, 50]

$$\begin{aligned} E\psi_{c;v}(\mathbf{k}) &= (E_{\mathbf{k}}^c - E_{\mathbf{k}}^v)\psi_{c;v}(\mathbf{k}) + \\ &+ \sum_{\mathbf{q}} V(\mathbf{k} - \mathbf{q}) \langle u_{\mathbf{k}}^c | u_{\mathbf{q}}^c \rangle \langle u_{\mathbf{q}}^v | u_{\mathbf{k}}^v \rangle \psi_{c;v}(\mathbf{q}), \end{aligned} \quad (5)$$

where $\psi_{c;v}(\mathbf{k})$ is the excitonic wave function that we wish to obtain, $|u_{\mathbf{k}}^{v/c}\rangle$ and $E_{\mathbf{k}}^{v/c}$ are the single particle electronic wave functions and energies, respectively, and $V(\mathbf{k})$ is an electrostatic potential coupling

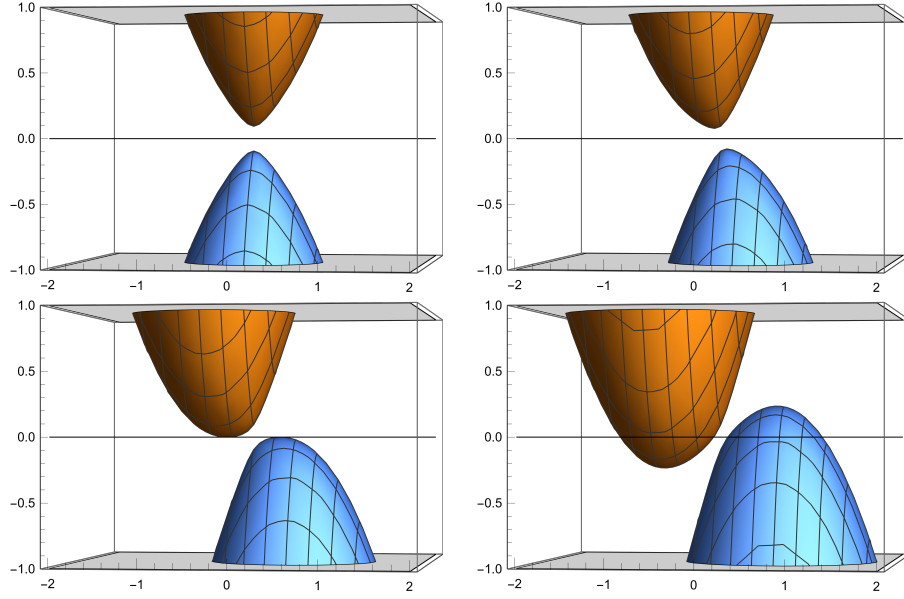


Figure 1. 3D plot of the band structure of the tilted Dirac Hamiltonian of Eq. (1) for $t/v = 0$ (top-left), $t/v = 0.5$ (top-right), $t/v = 1$ (bottom-left), and $t/v = 1.5$ (bottom-right). Labeled axes are the k_x axis (horizontal, in \AA^{-1}) and energy (vertical, in eV).

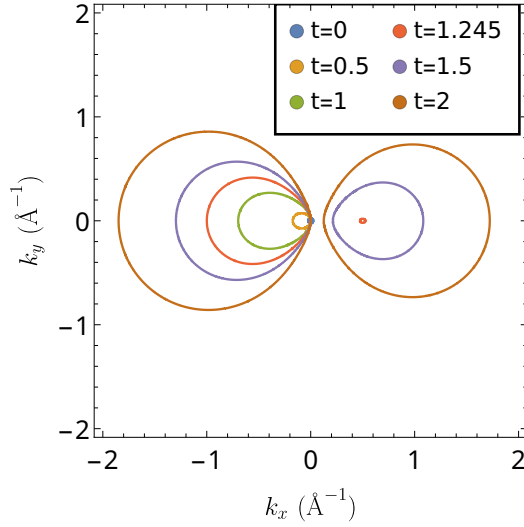


Figure 2. Fermi rings of the Hamiltonian of Eq. (1) at $E_F = m/2$ for various values of t/v . The rings associated with the conduction band are present on the left of the figure, while those associated with the valence bands are present on the right.

different bands and thus capturing many-body effects including the intrinsic many-body nature of excitons.

Assuming the excitons have a well-defined angular momentum ℓ , we can write their wave functions as $\psi_{c;v}(\mathbf{k}) = f_{c;v}(k) e^{i\ell\theta}$. Under this assumption, we can

write the BSE as

$$E f_{c;v}(k) e^{i\ell\theta_k} = (E_{\mathbf{k}}^c - E_{\mathbf{k}}^v) f_{c;v}(k) e^{i\ell\theta_k} + \sum_{\mathbf{q}} V(\mathbf{k} - \mathbf{q}) \langle u_{\mathbf{k}}^c | u_{\mathbf{q}}^c \rangle \langle u_{\mathbf{q}}^v | u_{\mathbf{k}}^v \rangle f_{c;v}(q) e^{i\ell\theta_q}. \quad (6)$$

Taking the thermodynamic limit and rearranging the complex exponentials, the Bethe-Salpeter equation is now given by

$$E f_{c;v}(k) = (E_{\mathbf{k}}^c - E_{\mathbf{k}}^v) f_{c;v}(k) - \int \frac{q dq d\theta_q}{4\pi^2} [V(\mathbf{k} - \mathbf{q}) * \langle u_{\mathbf{k}}^c | u_{\mathbf{q}}^c \rangle \langle u_{\mathbf{q}}^v | u_{\mathbf{k}}^v \rangle f_{c;v}(q) e^{i\ell(\theta_q - \theta_k)}]. \quad (7)$$

The process of solving the Bethe-Salpeter equation in monolayer and multilayer systems has been thoroughly discussed recently [51, 52], so we will not go into the details of the calculations.

We consider the electrostatic interaction to be given by the Rytova-Keldysh potential [53, 54], obtained by solving the Poisson equation for a charge embedded in a thin film of vanishing thickness. In momentum space, this potential is given by

$$V(\mathbf{k}) = 2\pi \frac{\hbar c \alpha}{\epsilon} \frac{1}{k(1 + r_0 k)}, \quad (8)$$

where $\alpha = 1/137$ is the fine-structure constant and ϵ the mean dielectric constant of the medium above/below the monolayer, here considered to be either hexagonal boron-nitride (hBN) or quartz. The parameter r_0 corresponds to an in-plane screening

length related to the 2D polarizability of the material. It can be calculated from the single particle Hamiltonian of the system[55], for $t < v$, as

$$r_0 = \frac{\hbar^3 c \alpha}{\pi m_0^2} \int \frac{|\langle u_{\mathbf{k}}^c | P_x | u_{\mathbf{k}}^v \rangle|^2}{[E_c(k) - E_v(k)]^3} k dk d\theta, \quad (9)$$

with m_0 the free electron mass, although *ab initio* calculations might be necessary for accurate computation of r_0 depending on the material[56].

3.2. Influence of the tilt parameter

When computing the momentum matrix element present in Eq. (9), a dependence on t is only present on its x component as

$$P_x = \frac{m_0}{\hbar} \frac{\partial}{\partial k_x} \hat{H}_d = \frac{m_0}{\hbar} \begin{bmatrix} t - 2k_x \alpha & -iv\eta \\ iv\eta & t + 2k_x \alpha \end{bmatrix}. \quad (10)$$

However, the diagonal terms proportional to t are canceled by the orthogonality relation of the two eigenvectors when $\langle u_{\mathbf{k}}^c | P_x | u_{\mathbf{k}}^v \rangle$ is computed. Explicitly, this term reads

$$e^{-i\theta} t [a_+^\dagger(k) a_-(k) + b_+^\dagger(k) b_-(k)] = 0, \quad (11)$$

with a_\pm and b_\pm the normalized spinor components of the eigenvectors in Eq. (4), written generically as

$$\begin{aligned} |u_+(k, \theta)\rangle &= \begin{bmatrix} a_+(k) \\ b_+(k) e^{i\theta} \end{bmatrix}, \\ |u_-(k, \theta)\rangle &= \begin{bmatrix} a_-(k) e^{-i\theta} \\ b_-(k) \end{bmatrix}. \end{aligned} \quad (12)$$

This cancellation, together with the fact that neither the difference of energy between the two bands nor the eigenvectors themselves depend on t , implies that the t parameter will not change the results obtained from solving the Bethe-Salpeter equation. As such, the obtained excitonic states will be independent of the tilt parameter t .

First considering the TMD encapsulated in hBN, the energies of first and second s -series states are, respectively, $E_{1s} = 134$ meV and $E_{2s} = 176$ meV. When $t \approx 1.1v$, the top of the valence band crosses the excitonic level, as shown in Fig. (3-a). This marks the onset of the instability against the spontaneous formation of excitons. Although the system is a semi-metal for this value of the ratio t/v , the carrier density is still very small, indicating that screening is still weak and the long-range character of the electron-hole interaction should be preserved.

By changing the material by which the TMD is encapsulated, it is possible to tune the exciton binding energy. For instance, by replacing hBN by quartz (whose relative dielectric constant is 3.8 [57]), the

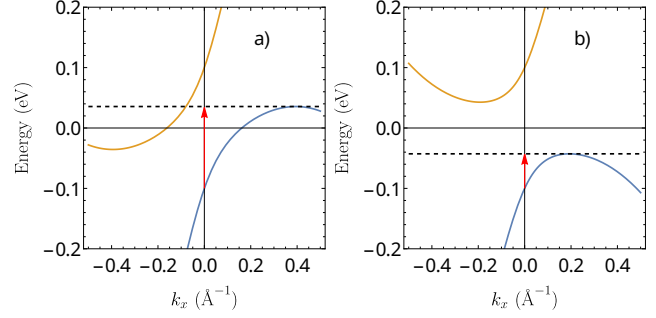


Figure 3. Band structure of the tilted model for two different values of the tilt parameter, $t = 1.1v$ (a) and $t = 0.83v$ (b). In each case we show the excitonic level (dashed lines) for different substrates, hBN (a) and quartz (b). The values chosen for t correspond to the onset of the excitonic instability for each case.

energy of the $1s$ exciton is $E_{1s} = 56.6$ meV. In this case, the onset of the excitonic instability happens for $t \approx 0.83v$, well into the semiconducting regime, as shown in Fig. (3-b). The fact that, for all $t \neq 0$, the gap is indirect, guarantees that the renormalization of the exciton binding energy and the dielectric function are small even for an arbitrarily small gap[41].

In Fig. (4) we plot the absolute value squared of the first two s -series excitonic wave functions where the TMD has been encapsulated in quartz. These plots are centered at $k = 0$ for a square region of side 20 \AA^{-1} .

3.3. Excitonic Conductivity

In the dipole approximation, and considering normal incidence, the optical conductivity is given by[48]

$$\sigma_{\alpha,\beta}^{(1)}(\hbar\omega) \propto \sum_n E_n \frac{\Omega_{n,\alpha} \Omega_{n,\beta}^*}{E_n - \hbar\omega - i\Gamma_n} + (\omega \rightarrow -\omega)^*, \quad (13)$$

where the sum over n represents the sum over excitonic states with energy E_n and wave function ψ_n , and Γ_n is a phenomenological broadening parameter considered to be n -dependent in a similar fashion as [51]. In Eq. (13), $\Omega_{n,\alpha}$ is defined as

$$\Omega_{n,\alpha} = \sum_{\mathbf{k}} \psi_n(\mathbf{k}) \langle u_{\mathbf{k}}^v | \mathbf{r}_\alpha | u_{\mathbf{k}}^c \rangle, \quad (14)$$

with $\langle u_{\mathbf{k}}^v | \mathbf{r}_\alpha | u_{\mathbf{k}}^c \rangle$ the interband dipole operator matrix element in the α direction, obtained using the relation

$$\langle u_{\mathbf{k}}^v | \mathbf{r}_\alpha | u_{\mathbf{k}}^c \rangle = \frac{\langle u_{\mathbf{k}}^v | [H, \mathbf{r}_\alpha] | u_{\mathbf{k}}^c \rangle}{E_k^v - E_k^c}. \quad (15)$$

Inserting this relation into Eq. (13), we then write the excitonic xx -conductivity as

$$\begin{aligned} \sigma_{xx}^{(1)}(\omega) &= \frac{e^2}{4\pi^2 i \hbar} \sum_n \frac{E_n \left| \int \psi_n(\mathbf{k}) \frac{\langle u_{\mathbf{k}}^v | [H, x] | u_{\mathbf{k}}^c \rangle}{E_k^v - E_k^c} k dk d\theta \right|^2}{E_n - (\hbar\omega + i\Gamma_n)} + \\ &+ (\omega \rightarrow -\omega)^*. \end{aligned} \quad (16)$$

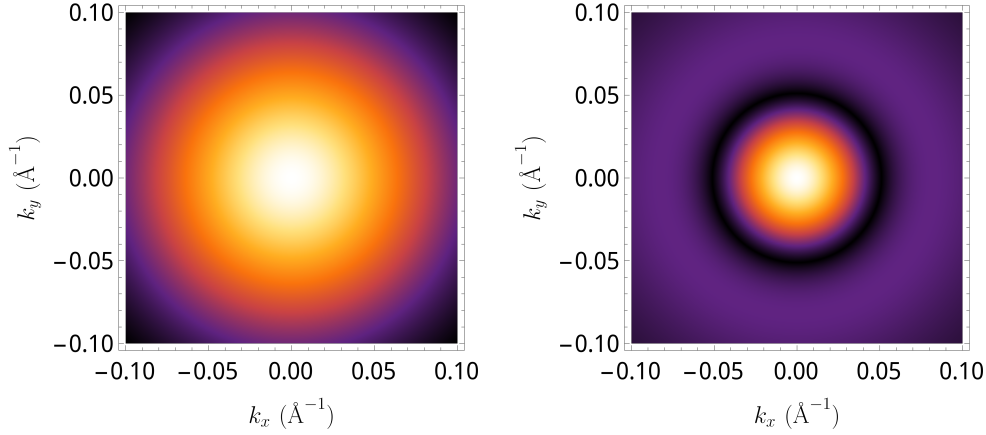


Figure 4. Absolute value squared of the wave functions of the two lowest energy excitonic s -series states centered at $k = 0$ considering the TMD encapsulated in quartz.

The optical selection rules are directly obtained from the phase factors of the single particle states in Eq. (12) when the commutator $\langle u_{\mathbf{k}}^v | [H, \mathbf{r}_\alpha] | u_{\mathbf{k}}^c \rangle$ is explicitly expanded. Recalling Eq. (10), as well as the discussion regarding eigenvector orthogonality that followed, the allowed transitions are associated with states with angular momentum $\ell = 0$ (s -series states) and $\ell = \pm 2$ (d -series states). Explicitly, the commutator reads

$$\langle u_{\mathbf{k}}^v | [H, x] | u_{\mathbf{k}}^c \rangle = \mathcal{A}(k) + \mathcal{B}(k) e^{-2i\theta}, \quad (17)$$

with $\mathcal{A}(k)$ and $\mathcal{B}(k)$ the radial dependence of both the spinor components and the numerical parameters in the momentum matrix of Eq. (10). These two functions are then given by

$$\begin{aligned} \mathcal{A}(k) &= -iv\eta a_+^\dagger(k) b_-(k) + \\ &\quad + k\alpha \left[b_+^\dagger(k) b_-(k) - a_+^\dagger(k) a_-(k) \right], \\ \mathcal{B}(k) &= iv\eta b_+^\dagger(k) a_-(k) + \\ &\quad + k\alpha \left[b_+^\dagger(k) b_-(k) - a_+^\dagger(k) a_-(k) \right]. \end{aligned} \quad (18)$$

To compare the oscillator strength of the two possible types of transitions, we compute the oscillator strength for d -series transitions as

$$|\Omega_{n,d;x}|^2 = \left| \int \frac{f_{n;d}(k) e^{2i\theta} \mathcal{B}(k) e^{-2i\theta}}{E_k^v - E_k^c} k dk d\theta \right|^2, \quad (19)$$

where $f_{n;d}(k)$ is the excitonic radial wave function for d -series states. On the other hand, the oscillator strength for s -series transitions is given by

$$|\Omega_{n,s;x}|^2 = \left| \int \frac{f_{n;s}(k) \mathcal{A}(k)}{E_k^v - E_k^c} k dk d\theta \right|^2, \quad (20)$$

where $f_{n;s}(k)$ is the excitonic radial wave function for s -series states. The first resonance for the $\ell = 2$

angular momentum series occurs at around 156 meV, and we obtain an oscillator strength around 2 orders of magnitude smaller than that of the s -series transitions closest to it.

In Fig. 5, we plot the real part of the excitonic xx -conductivity with a broadening parameter of $\Gamma = 3$ meV. In its inset, the contribution from d -series states is also plotted, magnified by a factor of 100 as to improve comparison of the oscillator strengths of both types of transitions.

4. Conclusions

We studied the properties of excitons in Janus TMD monolayers modeled by a tilted massive Dirac Hamiltonian. We have shown that, as the tilt parameter increases, the band gap is continuously suppressed, whereas the maximum of the valence band and the minimum of the conduction band shift in opposite directions along the tilting axis, making the gap indirect. Notably, the exciton binding energies remain unchanged as the tilting is enhanced. This means that the (indirect) gap can be made smaller than the exciton binding, a situation that has been predicted to lead to an excitonic instability, and possibly the formation of an excitonic insulator phase.

Finally, we also considered the excitonic linear conductivity, discussing the optical selection rules for the system. With the model Hamiltonian considered, only states with angular momentum $\ell = 0$ or $|\ell| = 2$ can be excited, with the resonances associated with $\ell = 0$ transitions more than two orders of magnitude greater than those associated with $\ell = \pm 2$ transitions. As expected from the solutions of the Bethe-Salpeter equation, the excitonic linear conductivity was also fully independent of the tilt parameter, even when comparing light polarized in

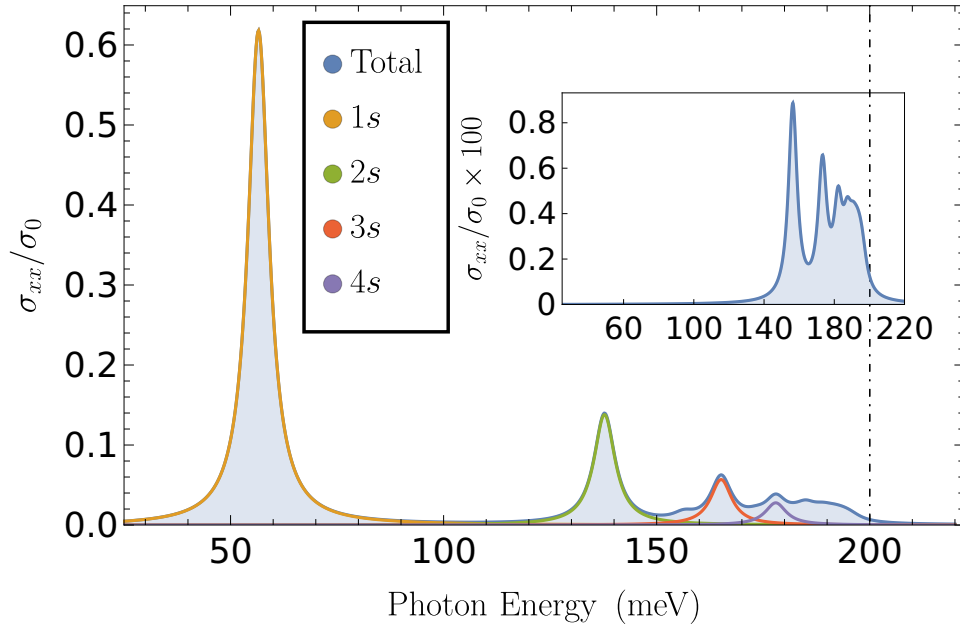


Figure 5. Real part of the excitonic xx -conductivity for a material described by a tilted Dirac Hamiltonian encapsulated in quartz with broadening parameter $\Gamma = 3$ meV, and a $N = 450$ point Gauss-Legendre quadrature. First ten states of each excitonic series were considered for the total conductivity. Vertical dashed lines represent the bandgap of the system. The conductivity is given in units of the conductivity of monolayer graphene $\sigma_0 = e^2/4h$. In the inset, we plot the contribution from only d -series states scaled by two orders of magnitude to improve readability and comparison of the relative intensity. The vertical dashed line representing the bandgap has been aligned by the same value in both the main plot and the inset.

either the parallel or the perpendicular direction of the tilt axis. Importantly, the excitonic contribution to the conductivity is insensitive to the value of the tilting parameter t . As the system is pushed towards the excitonic instability by tuning t , one can expect $\sigma_{xx}(\omega)$ to remain unchanged until the system reaches the instability point, where $\sigma_{xx}(\omega)$ is expected to change abruptly, marking the onset of the phase change.

Acknowledgements

We acknowledge fruitful discussions with Joaquín Fernández-Rossier and Gonalo Catarina. M. F. C. M. Q. acknowledges the International Nanotechnology Laboratory (INL) and the Portuguese Foundation for Science and Technology (FCT) for the Quantum Portugal Initiative (QPI) grant SFRH/BD/151114/2021. N. M. R. P. acknowledges support by the Portuguese Foundation for Science and Technology (FCT) in the framework of the Strategic Funding UIDB/04650/2020, COMPETE 2020, PORTUGAL 2020, FEDER, and FCT through projects POCI-01-0145-FEDER-028114, POCI-01-0145-FEDER-02888 and PTDC/NANOPT/29265/2017, PTDC/FIS-MAC/2045/2021, EXPL/FIS-MAC/0953/2021, and from the European Commission through the project Graphene Driven Revolutions in ICT and Beyond (Ref. No. 881603, CORE 3).

References

- [1] Ang-Yu Lu, Hanyu Zhu, Jun Xiao, Chih-Piao Chuu, Yimo Han, Ming-Hui Chiu, Chia-Chin Cheng, Chih-Wen Yang, Kung-Hwa Wei, Yiming Yang, Yuan Wang, Dimosthenis Sokaras, Dennis Nordlund, Peidong Yang, David A. Muller, Mei-Yin Chou, Xiang Zhang, and Lain-Jong Li. Janus monolayers of transition metal dichalcogenides. *Nature Nanotechnology*, 12(8):744–749, Aug 2017.
- [2] Jing Zhang, Shuai Jia, Iskandar Kholmanov, Liang Dong, Dequan Er, Weibing Chen, Hua Guo, Zehua Jin, Vivek B. Shenoy, Li Shi, and Jun Lou. Janus monolayer transition-metal dichalcogenides. *ACS Nano*, 11(8):8192–8198, Aug 2017.
- [3] Anders Christian Riis-Jensen. *Computational Studies of Two-Dimensional Materials and Heterostructures*. PhD thesis, 2020.
- [4] Ting Zheng, Yu-Chuan Lin, Yiling Yu, Pavel Valencia-Acuna, Alexander A. Puretzky, Riccardo Torsi, Chenze Liu, Ilia N. Ivanov, Gerd Duscher, David B. Geohegan, Zhenhua Ni, Kai Xiao, and Hui Zhao. Excitonic dynamics in janus mosse and wsse monolayers. *Nano Letters*, 21(2):931–937, 2021. PMID: 33405934.
- [5] Xiao Tang and Liangzhi Kou. 2d janus transition metal dichalcogenides: Properties and applications. *physica status solidi (b)*, 259(4):2100562, 2022.
- [6] Cheng-gong Zhang, Di-di Zhao, Wei-xiao Ji, Chang-wen Zhang, and Pei-Ji Wang. Monolayer nbnse with high fermi velocity and anisotropic properties. *physica status solidi (b)*, 259(4):2100440, 2022.
- [7] Liang Dong, Jun Lou, and Vivek B. Shenoy. Large in-plane and vertical piezoelectricity in janus transition metal dichalcogenides. *ACS Nano*, 11(8):8242–8248, Aug 2017.
- [8] Jian Liu and Sokrates T. Pantelides. Mechanisms of

- pyroelectricity in three- and two-dimensional materials. *Phys. Rev. Lett.*, 120:207602, May 2018.
- [9] Tao Hu, Fanhao Jia, Guodong Zhao, Jiongyao Wu, Alessandro Stroppa, and Wei Ren. Intrinsic and anisotropic rashba spin splitting in janus transition-metal dichalcogenide monolayers. *Phys. Rev. B*, 97:235404, Jun 2018.
- [10] Hao Jin, Tao Wang, Zhi-Rui Gong, Chen Long, and Ying Dai. Prediction of an extremely long exciton lifetime in a janus-moste monolayer. *Nanoscale*, 10:19310–19315, 2018.
- [11] Xiangchao Ma, Xin Wu, Haoda Wang, and Yucheng Wang. A janus mosse monolayer: a potential wide solar-spectrum water-splitting photocatalyst with a low carrier recombination rate. *J. Mater. Chem. A*, 6:2295–2301, 2018.
- [12] Cui Jin, Xiao Tang, Xin Tan, Sean C. Smith, Ying Dai, and Liangzhi Kou. A janus mosse monolayer: a superior and strain-sensitive gas sensing material. *J. Mater. Chem. A*, 7:1099–1106, 2019.
- [13] M. Idrees, H. U. Din, R. Ali, G. Rehman, T. Hussain, C. V. Nguyen, Iftikhar Ahmad, and B. Amin. Optoelectronic and solar cell applications of janus monolayers and their van der waals heterostructures. *Phys. Chem. Chem. Phys.*, 21:18612–18621, 2019.
- [14] Michael Victor Berry. Quantal phase factors accompanying adiabatic changes. *Proceedings of the Royal Society of London. A. Mathematical and Physical Sciences*, 392(1802):45–57, March 1984.
- [15] Di Xiao, Ming-Che Chang, and Qian Niu. Berry phase effects on electronic properties. *Rev. Mod. Phys.*, 82:1959–2007, Jul 2010.
- [16] Inti Sodemann and Liang Fu. Quantum nonlinear hall effect induced by berry curvature dipole in time-reversal invariant materials. *Phys. Rev. Lett.*, 115:216806, Nov 2015.
- [17] Nesta Benno Joseph, Saswata Roy, and Awadhesh Narayan. Tunable topology and berry curvature dipole in transition metal dichalcogenide janus monolayers. *Materials Research Express*, 8(12):124001, dec 2021.
- [18] Z. Z. Du, C. M. Wang, Hai-Zhou Lu, and X. C. Xie. Band signatures for strong nonlinear hall effect in bilayer wte₂. *Phys. Rev. Lett.*, 121:266601, Dec 2018.
- [19] Sten Haastrup, Mikkel Strange, Mohnish Pandey, Thorsten Deilmann, Per S Schmidt, Nicki F Hinsche, Morten N Gjerding, Daniele Torelli, Peter M Larsen, Anders C Riis-Jensen, Jakob Gath, Karsten W Jacobsen, Jens Jørgen Mortensen, Thomas Olsen, and Kristian S Thygesen. The computational 2d materials database: high-throughput modeling and discovery of atomically thin crystals. *2D Materials*, 5(4):042002, sep 2018.
- [20] A. D. Zabolotskiy and Yu. E. Lozovik. Strain-induced pseudomagnetic field in the dirac semimetal borophene. *Phys. Rev. B*, 94:165403, Oct 2016.
- [21] Sonu Verma, Alestin Mawrie, and Tarun Kanti Ghosh. Effect of electron-hole asymmetry on optical conductivity in 8-*pmmn* borophene. *Phys. Rev. B*, 96:155418, Oct 2017.
- [22] J. C. Sandoval-Santana, V. G. Ibarra-Sierra, A. Kunold, and Gerardo G. Naumis. Floquet spectrum for anisotropic and tilted dirac materials under linearly polarized light at all field intensities. *Journal of Applied Physics*, 127(23):234301, 2020.
- [23] Abdel E. Champo and Gerardo G. Naumis. Metal-insulator transition in 8-*pmmn* borophene under normal incidence of electromagnetic radiation. *Phys. Rev. B*, 99:035415, Jan 2019.
- [24] Saúl A. Herrera and Gerardo G. Naumis. Kubo conductivity for anisotropic tilted dirac semimetals and its application to 8-*pmmn* borophene: Role of frequency, temperature, and scattering limits. *Phys. Rev. B*, 100:195420, Nov 2019.
- [25] Masao Ogata, Soshun Ozaki, and Hiroyasu Matsuura. Anomalous spin transport properties of gapped dirac electrons with tilting. *Journal of the Physical Society of Japan*, 91(2):023708, 2022.
- [26] Lukas Muechler, A. Alexandradinata, Titus Neupert, and Roberto Car. Topological nonsymmorphic metals from band inversion. *Phys. Rev. X*, 6:041069, Dec 2016.
- [27] Jing Li, Tian Xu, Guo-Bao Zhu, and Hui Pan. Photoinduced anomalous hall and nonlinear hall effect in borophene. *Solid State Communications*, 322:114092, 2020.
- [28] Habib Rostami and Vladimir Juričić. Probing quantum criticality using nonlinear hall effect in a metallic dirac system. *Phys. Rev. Research*, 2:013069, Jan 2020.
- [29] Daigo Ohki, Michihiro Hirata, Takehiro Tani, Kazushi Kanoda, and Akito Kobayashi. Chiral excitonic instability of two-dimensional tilted dirac cones. *Phys. Rev. Research*, 2:033479, Sep 2020.
- [30] Meng-Xue Guan, En Wang, Pei-Wei You, Jia-Tao Sun, and Sheng Meng. Manipulating weyl quasiparticles by orbital-selective photoexcitation in wte₂. *Nature Communications*, 12(1):1885, Mar 2021.
- [31] Stephen M. Winter, Kira Riedl, and Roser Valentí. Importance of spin-orbit coupling in layered organic salts. *Phys. Rev. B*, 95:060404, Feb 2017.
- [32] Toshihito Osada. Topological insulator state due to finite spin-orbit interaction in an organic dirac fermion system. *Journal of the Physical Society of Japan*, 87(7):075002, 2018.
- [33] Takahiro Morimoto and Naoto Nagaosa. Topological nature of nonlinear optical effects in solids. *Science Advances*, 2(5):e1501524, 2016.
- [34] Yang Gao and Bin Ge. Second harmonic generation in dirac/weyl semimetals with broken tilt inversion symmetry. *Opt. Express*, 29(5):6903–6914, Mar 2021.
- [35] Victor Pardo and Warren E. Pickett. Half-metallic semi-dirac-point generated by quantum confinement in tio₂/vo₂ nanostructures. *Phys. Rev. Lett.*, 102:166803, Apr 2009.
- [36] Huaqing Huang, Zhirong Liu, Hongbin Zhang, Wenhui Duan, and David Vanderbilt. Emergence of a chern-insulating state from a semi-dirac dispersion. *Phys. Rev. B*, 92:161115, Oct 2015.
- [37] Kush Saha. Photoinduced chern insulating states in semi-dirac materials. *Phys. Rev. B*, 94:081103, Aug 2016.
- [38] Jin-Na Chen, Yan-Yan Yang, Yong-Long Zhou, Yong-Jia Wu, Hou-Jian Duan, Ming-Xun Deng, and Rui-Qiang Wang. Photon-modulated linear and nonlinear anomalous hall effects in type-ii semi-dirac semimetals. *Phys. Rev. B*, 105:085124, Feb 2022.
- [39] Yang Zhang, Jeroen van den Brink, Claudia Felser, and Binghai Yan. Electrically tuneable nonlinear anomalous hall effect in two-dimensional transition-metal dichalcogenides WTe₂ and MoTe₂. *2D Materials*, 5(4):044001, jul 2018.
- [40] N. F. Mott. The transition to the metallic state. *The Philosophical Magazine: A Journal of Theoretical Experimental and Applied Physics*, 6(62):287–309, 1961.
- [41] Jacques Des Cloizeaux. Exciton instability and crystallographic anomalies in semiconductors. *Journal of Physics and Chemistry of Solids*, 26(2):259–266, 1965.
- [42] W. Kohn. Excitonic phases. *Phys. Rev. Lett.*, 19:439–442, Aug 1967.
- [43] D. Jérôme, T. M. Rice, and W. Kohn. Excitonic insulator. *Phys. Rev.*, 158:462–475, Jun 1967.
- [44] B.I. Halperin and T.M. Rice. The excitonic state at the semiconductor-semimetal transition**a summary

- of thin paper was presented at the meeting of the american physical society, at toronto, canada, june 1967. volume 21 of *Solid State Physics*, pages 115–192. Academic Press, 1968.
- [45] Robert S. Knox. *Theory of excitons*. Number 5 in Solid state physics Supplement. Academic Press, New York, 1. print edition, 1963.
 - [46] Shun-Qing Shen. *Topological Insulators*. Springer Berlin Heidelberg, 2012.
 - [47] Alireza Taghizadeh and T. G. Pedersen. Nonlinear optical selection rules of excitons in monolayer transition metal dichalcogenides. *Phys. Rev. B*, 99:235433, Jun 2019.
 - [48] Thomas Garm Pedersen. Intraband effects in excitonic second-harmonic generation. *Phys. Rev. B*, 92:235432, Dec 2015.
 - [49] Ting Cao, Meng Wu, and Steven G. Louie. Unifying optical selection rules for excitons in two dimensions: Band topology and winding numbers. *Phys. Rev. Lett.*, 120:087402, Feb 2018.
 - [50] Santosh Kumar Radha, Walter R. L. Lambrecht, Brian Cunningham, Myrta Grüning, Dimitar Pashov, and Mark van Schilfgaarde. Optical response and band structure of LiCoO₂ including electron-hole interaction effects. *Phys. Rev. B*, 104:115120, Sep 2021.
 - [51] J. C. G. Henriques, Itai Epstein, and N. M. R. Peres. Absorption and optical selection rules of tunable excitons in biased bilayer graphene. *Phys. Rev. B*, 105:045411, Jan 2022.
 - [52] M. F. C. Martins Quintela, J. C. G. Henriques, Luiz G. M. Tenório, and Nuno Miguel Machado Reis Peres. Theoretical methods for excitonic physics in two-dimensional materials. *physica status solidi (b)*, April 2022.
 - [53] S. N. Rytova. The screened potential of a point charge in a thin film. *Mosc. Un. Phys. Bul.*, 22(30), 1967.
 - [54] L. V. Keldysh. Coulomb interaction in thin semiconductor and semimetal films. *Sov. J. Exp. and Theor. Phys. Lett.*, 29:658, 1979.
 - [55] Pengke Li and Ian Appelbaum. Excitons without effective mass: Biased bilayer graphene. *Phys. Rev. B*, 99:035429, Jan 2019.
 - [56] Tian Tian, Declan Scullion, Dale Hughes, Lu Hua Li, Chih-Jen Shih, Jonathan Coleman, Manish Chhowalla, and Elton J. G. Santos. Electronic polarizability as the fundamental variable in the dielectric properties of two-dimensional materials. *Nano Letters*, 20(2):841–851, 2020. PMID: 31888332.
 - [57] R.A. Serway, J.S. Faughn, and C.J. Moses. *College Physics*. Number vol. 1 in College Physics. Brooks/Cole, 2003.